

# Structure of a left-handed DNA G-quadruplex

Wan Jun Chung<sup>1</sup>, Brahim Heddi<sup>1</sup>, Emmanuelle Schmitt<sup>2</sup>, Kah Wai Lim<sup>1</sup>, Yves Mechulam<sup>2</sup> and Anh Tuân Phan<sup>1,\*</sup>

<sup>1</sup>School of Physical and Mathematical Sciences, Nanyang Technological University, Singapore 637371, Singapore<sup>2</sup>Laboratoire de Biochimie, CNRS UMR7654, Ecole Polytechnique, Palaiseau 91128, France

Submitted to Proceedings of the National Academy of Sciences of the United States of America

**Aside from the well-known double helix, DNA can also adopt an alternative four-stranded structure known as G-quadruplex. Implications of such a structure in cellular processes, as well as its therapeutic and diagnostic applications, have been reported. The G-quadruplex structure is highly polymorphic, but so far only right-handed helical forms have been observed. Here we present the first NMR and X-ray structures of a left-handed DNA G-quadruplex. The structure displays unprecedented features that can be exploited as unique recognition elements.**

G-quadruplex | left-handed helix | nucleic acid | NMR | X-ray crystallography

## INTRODUCTION

DNA can adopt diverse structural conformations (1-9), ranging from double helical A-, B- and Z-forms, to triplexes, quadruplexes, and branched architectures. Different DNA conformations have been associated with different biological functions (1, 2, 6, 7, 9). While the canonical double helix (1) (B-DNA) and most other structural forms follow a right-handed helical twist, Z-DNA is the only left-handed form of DNA (2) known to date.

Recent mounting biological interest have driven attention to G-quadruplex (G4) (10-16), a four-stranded structure consisting of a stack of G-tetrad layers, each comprising four guanines Hoogsteen hydrogen-bonded in a coplanar arrangement (17). This helical structure with different possible orientations between the four strands is highly polymorphic (6, 7, 16, 18, 19), but so far only right-handed forms have been observed. G4-forming sequences are found in numerous regions of the human genome (16). Recent studies demonstrated their existence in human cells (15) and their involvement in cellular regulation including recombination (12), replication (13, 14), transcription (10) and translation (11). On the other hand, synthetic G4s have been introduced as unique structural elements in nanotechnology (20) as well as aptamers for therapeutic and diagnostic purposes (21). For instance, the G-rich oligonucleotide *AGRO100* (SI Appendix, Table S1) has been shown to exhibit potent anti-proliferative activity against a range of cancer cells (21) and was later found to adopt multiple G4 conformations (22).

Herein we present NMR and X-ray structures of a G4 derived from *AGRO100*, adopted by the sequence d[T(GGT)<sub>4</sub>TG(TGG)<sub>3</sub>TGTT] (henceforth denoted as *Z-G4*), which exhibits distinct circular dichroism (CD) profile with a negative peak at ~275 nm and a positive peak at ~250 nm (Figure 1b), nearly inverted from that of the right-handed G4 topologies reported to date (23). The unprecedented left-handed helical twist of *Z-G4*, as presented below, explains its atypical CD signals.

## RESULTS AND DISCUSSION

Imino proton NMR spectrum of *Z-G4* in solution containing ~100 mM K<sup>+</sup> showed sixteen major sharp peaks between 10.6–11.8 ppm (Figure 1a), indicative of the formation of a four-layered G4. The NMR solution structure of *Z-G4* was elucidated (Table 1 and Figure 2a) based on rigorous assignment approaches using site-specific isotopic labels and through-bond correlation experiments (SI Appendix, Table S2 and Figs S1 and S2), largely following protocols described previously (18). The structure in-

volves two continuous stacked G4 blocks (Figure 2c), each comprising two G-tetrad layers arranged in the same hydrogen-bond directionalities (G2•G5•G8•G11 and G3•G6•G9•G12 for the top G4 block, G15•G18•G21•G24 and G17•G20•G23•G26 for the bottom G4 block) (SI Appendix, Fig. S3), connected through a central linker (T13–T14). All guanine residues adopt the *anti* glycosidic conformation with the exception of G2, which is in the *syn* conformation.

*Z-G4* was successfully crystallized in the presence of potassium ions, using methylpentanediol (MPD) as precipitating agent. Crystals belonged to the P3<sub>2</sub>21 group and diffracted to 1.5 Å resolution. The structure was solved by molecular replacement, using the NMR solution structure as a starting model, and refined to 1.5 Å resolution (*R*-factor=14.1%; *R*<sub>free</sub>=18%; Table 2 and Figure 2b). Head-to-head and tail-to-tail crystal packing was observed, facilitated by thymine residues from the loops as well as by a potassium ion. Because of the head-to-head arrangement, two symmetry-related potassium ions are actually sandwiched between the two DNA molecules (SI Appendix, Fig. S4a). A hexacoordinated Mg<sup>2+</sup> ion is also involved in crystal packing (SI Appendix, Fig. S4b). Similar to typical right-handed G4s, three potassium ions are visible in the core, sandwiched between the G-tetrads. Finally, 94 ordered water molecules are located mainly within the grooves and along the phosphate backbone of *Z-G4*. Electron densities, attributed to water molecules, were observed at the 5'- and 3'-ends of the G-tetrad core (Figure 2b). However, the possibility of ions with low occupancy could not be excluded. Comparison between the NMR solution and X-ray crystal structures of *Z-G4* showed a high degree of concordance (pairwise r.m.s.d. of (1.63 ± 0.34) Å, excluding the last two residues) (SI Appendix, Fig. S5).

The strand arrangement of *Z-G4* conforms to that of a regular parallel-stranded G-tetrad core (Figure 2c), with stacking distance between successive G-tetrads having an average helical rise

### Significance

**Aside from double helical A-, B- and Z-forms, DNA can also adopt an alternative four-stranded structure known as G-quadruplex. Therapeutic and diagnostic applications of G-quadruplex as aptamers have been reported, in addition to their putative association with cellular processes. Here we present the NMR and X-ray structures of a left-handed DNA G-quadruplex derived from an aptameric G-rich oligonucleotide. The structure exhibits a left-handed helical twist with unprecedented features that can be exploited as unique recognition elements.**

### Reserved for Publication Footnotes

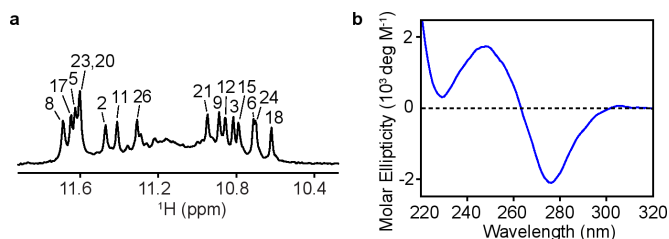


Fig. 1. (a) 1D imino proton NMR spectrum of Z-G4. (b) CD spectrum of Z-G4.

Table 1.

Table 1. NMR restraints and structure statistics		
<b>NMR restraints</b>		
Distance restraints	Exchangeable	Non-exchangeable
<b>DNA restraints</b>		
Intra-residue	3	310
Inter-residue	105	246
<b>Other Restraints</b>		
Hydrogen-bond restraints	64	
<b>Structure statistics</b>		
NOE violations		
Numbers (>0.2 Å)	0.500 ± 0.671	
Deviations from standard geometry		
Bond length (Å)	0.005 ± 0.000	
Bond angle (°)	0.800 ± 0.013	
Impropers (°)	0.448 ± 0.024	
Pairwise all heavy atom r.m.s.d. values (Å)		
All heavy atoms	1.950 ± 0.250	
G-tetrad core	1.089 ± 0.137	

of (3.46 ± 0.07) Å. Dimension of all four grooves (as defined by phosphate-to-phosphate distance between adjacent tetrad guanine residues) for the two G4 blocks is of medium width (~16.5 Å). The two G4 blocks are stacked through the G3•G6•G9•G12 and G15•G18•G21•G24 tetrads, consistent with the slower rate of solvent exchange of the imino protons in these tetrads as observed by NMR (SI Appendix, Fig. S6). Across the stacking interface, there is partial overlap between the five- and six-membered rings of the guanine bases from the two tetrad layers (between G3/G24, G12/G15, G9/G18 and G6/G21, respectively) (SI Appendix, Fig. S7a). Such stacking arrangements have previously been observed across various stacked G4 structures (24) (SI Appendix, Fig. S7b). However, as opposed to that observed in right-handed G4 structures, O4' atoms of the sugar residues in Z-G4 point in the direction of the strand progression (SI Appendix, Figs. S8a and S8b).

Within each G4 block, strands are connected by single-nucleotide thymine loops (T4, T7 and T10 for the top G4 block; T16, T19, T22 and T25 for the bottom G4 block). The backbone configuration of these loops deviates from that of a typical single-nucleotide propeller loop (25). Instead of flipping outwards, thymine bases T7, T10, T13, T16, T19, T22 and T25 collapse onto the terminal G-tetrads, allowing the O4' atoms of these residues to establish a hydrogen bond with the amino protons of the nearby tetrad guanine bases (G5, G8, G11, G26, G17, G20 and G23, respectively) (Figure 3 and SI Appendix, Fig. S9a,c). In the crystal structure, the relatively low B-values of these thymines (ranging between 13.4 and 17.2 Å<sup>2</sup> for T7, T10, T13, T22 and T25; 27.4 Å<sup>2</sup> for T16 and 22.6 Å<sup>2</sup> for T19), only slightly higher than the mean B-value of guanines in the G-tetrad core (13.6 Å<sup>2</sup>), indicated that

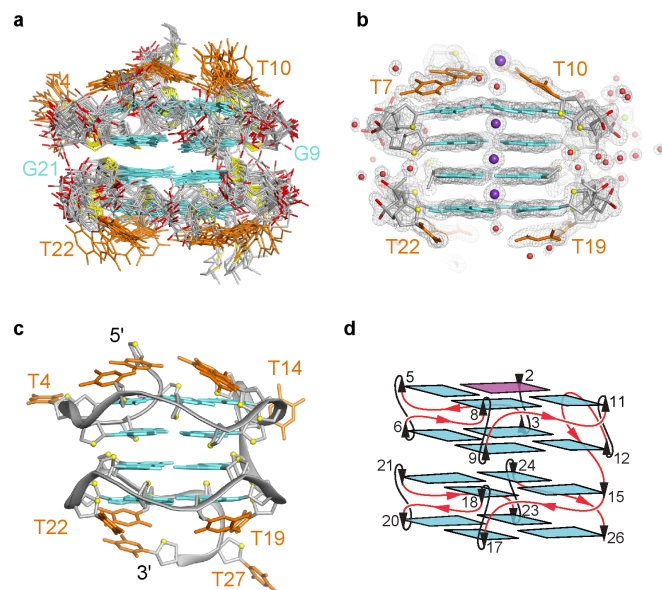


Fig. 2. (a) Ten lowest-energy superimposed solution structures of Z-G4. (b) Crystal structure of Z-G4. The electron density corresponds to the final 2mFo-DFc map contoured at 1.0 σ (c) Ribbon view of the crystal structure of Z-G4. Anti and syn guanine bases are colored in cyan and magenta, respectively; thymine bases, orange; phosphate backbone, grey; phosphate oxygens, red; O4' oxygens, yellow. Potassium ions and water molecules are colored in purple and red, respectively. (d) Schematic structure of Z-G4. Arrows represent the 5'-to-3' strand progression.

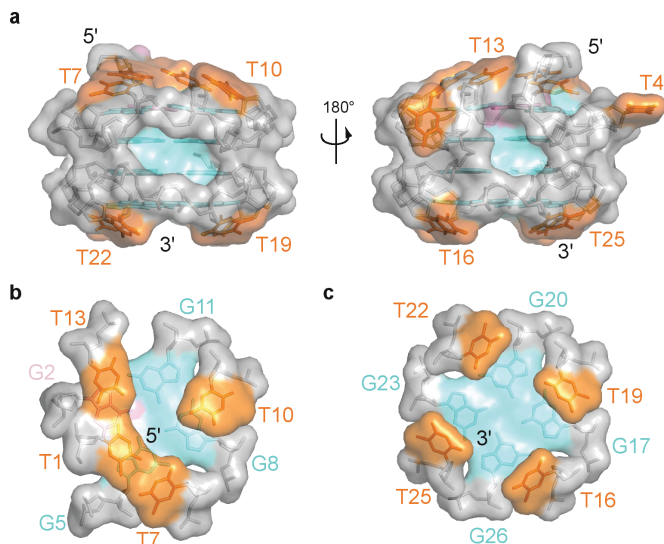
Table 2.

Table 2. Data collection and refinement statistics for structure determination.	
	Z-G4 <sup>a</sup>
<b>Data collection</b>	
Space group	P3 <sub>2</sub> 21
Cell dimensions	
a, b, c (Å)	51.90, 51.90, 40.17
α, β, γ (°)	90.0, 90.0, 120.0
Resolution (Å)	44.9 - 1.5
R <sub>sym</sub>	0.083 (0.642) <sup>b</sup>
I / σI	18.50 (2.76)
Completeness (%)	95.7 (77.7)
Redundancy	9.2 (5.6)
<b>Refinement</b>	
Resolution (Å)	44.9 - 1.5
Number of reflections	9875
R <sub>work</sub> / R <sub>free</sub>	0.1410/0.1800
Number of atoms	
DNA	631
K <sup>+</sup>	4
Mg <sup>2+</sup>	1
Water	94
B-factors (Å <sup>2</sup> )	DNA 16.81 K <sup>+</sup> 10.22 Mg <sup>2+</sup> 35.63 Water 31.66
r.m.s.d.	
Bond lengths (Å)	0.008
Bond angles (°)	1.090

<sup>a</sup>A single crystal was used for data collection.

<sup>b</sup>Values in parentheses are for highest-resolution shell.

these residues were well ordered. These structural arrangements are supported by the slow rate of exchange of the guanine amino



**Fig. 3.** Surface representation showing the capping of the top and bottom tetrad. (a) Side view. (b) Top view. (c) Bottom view. Guanine and thymine residues are colored in cyan and orange respectively. Phosphate backbone is colored in grey. Bases are labeled with their corresponding residue numbers.

protons as observed by NMR (SI Appendix, Fig. S9b,c). We also note alternative structural conformations for residues T4, G5 and T10. The accessible grooves and the capping of both G-tetrad ends by the thymines create a unique structural motif that could potentially serve as specific recognition element (Figure 3).

All taken together, general characteristics (*e.g.* tetrad geometry, groove dimensions, stacking distances) of *Z-G4* complies with those of a regular right-handed G4. However, backbone progression of successive guanine residues constituting each individual G4 block is left-handed (Figure 4a,e), which is reverse of that of a typical all-parallel-stranded G4 scaffold (*e.g.* monomeric three-layered G4 formed by the sequence  $d[TT(GGGT)_4]$ , henceforth denoted as *T95-2T*; SI Appendix Table S1 and Figure 4b,f) (25). Looking down each G4 block from 5' to 3', the oligonucleotide strand progresses in an anticlockwise manner for *Z-G4* (Figure 4c), in contrast to *T95-2T*, in which the oligonucleotide strand progresses in a clockwise manner (Figure 4d). On average, the relative rotation/twist between two successive guanine bases is reverse,  $(-25.73 \pm 2.00)^\circ$  for *Z-G4* vs.  $(+29.41 \pm 2.45)^\circ$  for *T95-2T* (Figure 4g,h). Such helical geometries are reflected by their contrasting CD spectra (SI Appendix, Fig. S10), which are almost mirror image of one another. Similar contrasting behavior was previously reported between *Z-DNA* and *B-DNA* (26). Analysis of the backbone dihedrals for *Z-G4* revealed a unique left turn:  $\zeta$  and  $(\beta+1)$  angles for the dinucleotide steps G5–G6, G8–G9, G11–G12, G17–G18, G20–G21 and G23–G24 approximate those observed in *Z-DNA* (which would have largely accounted for the left-handed progression of the G4 block), while  $(\alpha+1)$  angles approximate those observed in *B-DNA* (Table 3). Furthermore, a similar *Z-DNA*-like backbone configuration can be observed for the G2–G3 step of *Z-G4* (SI Appendix, Fig. S11). Such unusual local backbone conformations have recently been observed to occur in RNA quadruplex aptamers (27–29). Previously, quadruplexes with left-handed helicity have been artificially induced through partial or full incorporation of  $L$ -nucleotides (30, 31).

NMR and CD spectra showed that *Z-G4* adopted the same left-handed G4 scaffold under near-physiological ionic condition (SI Appendix, Fig. S12), but not in a  $Li^+$ -containing buffer, pointing towards the role of  $K^+$  ions in the stabilization of the G-tetrad core. CD experiments (SI Appendix, Fig. S13) showed that the *Z-G4* structure was formed under different  $K^+$  concentrations (ranging from 10 to 700 mM), and that its thermal stability in-

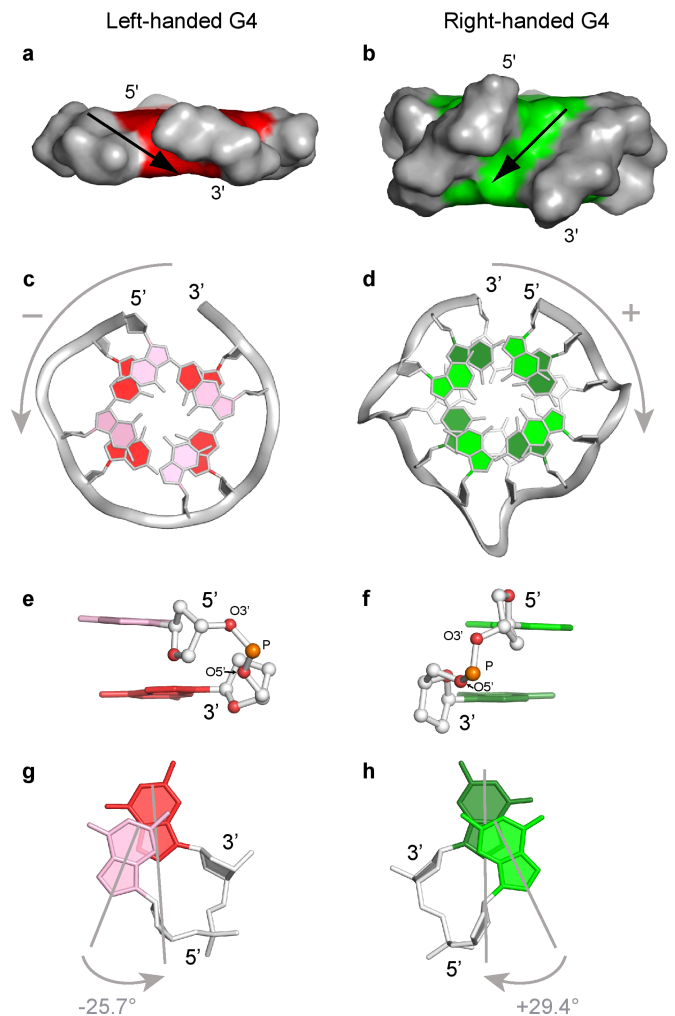


**Fig. 4.** (a) Surface representation of one block (two-layer tetrad) of *Z-G4* showing the left-handed directionality of the phosphate backbone. (b) Surface representation of *T95-2T* (PDB code, 2LK7) (three-layer tetrad) showing the right-handed directionality of the phosphate backbone. Thymine residues are removed for clarity. (c) Top view from the 5' end of *Z-G4* showing the anti-clockwise progression of the backbone, as depicted by the grey arrow. (d) Top view from the 5' end of *T95-2T* showing the clockwise progression of the backbone, as depicted by the grey arrow. (e) Side view of a representative dinucleotide step of *Z-G4*. (f) Side view of a representative dinucleotide step of *T95-2T*. (g) (Top view) G-tetrad stacking within subunit of *Z-G4* with a relative rotation of  $-25.7^\circ$ . (h) (Top view) G-tetrad stacking within monomeric unit of *T95-2T* with a relative rotation of  $+29.4^\circ$ .

creased with increasing  $K^+$  concentration (melting temperature,  $T_m \sim 45^\circ C$  at 90 mM  $K^+$ ;  $T_m \sim 62^\circ C$  at 700 mM  $K^+$ ). Sequence modifications on the central linker T13-T14 (*e.g.* reduction to one or zero nucleotides, or extension to four nucleotides) and on the first loop T4 (*e.g.* T-to-A, T-to-C, and T-to-TT) were well tolerated (SI Appendix, Table S3 and Fig. S14). Modifications at both ends, resulting in *AGRO100* (SI Appendix, Table S1), could also be tolerated, as observed from the similarity between the NMR and CD spectra of *Z-G4* and those of one isolated fraction of *AGRO100* (22).

The left-handed helical nature of *Z-G4* gives rise to a unique G4 scaffold featuring several unprecedented structural motifs, which could serve as natural or artificial recognition elements. Sequence matches of *Z-G4* were found in various locations of the human genome (SI Appendix, Table S3), while results from sequence modifications suggested scope for expanding the sequence definition of such a left-handed G-quadruplex structure.

**Table 3. Comparison of backbone torsion angles of Z-G4 with various right- and left-handed DNA forms.**

Backbone Dihedral	Quadruplex		Duplex	B-DNA <sup>d</sup>
	Z-G4 <sup>a</sup>	Regular G4 <sup>b</sup>	Z-DNA <sup>c</sup> <i>anti-syn</i> / <i>syn-anti</i>	
$\epsilon$	(316 ± 2)°	(197 ± 9)°	(267 ± 9)° / (240 ± 9)°	(184 ± 11)°
$\zeta$	(86 ± 3)°	(250 ± 10)°	(75 ± 9)° / (301 ± 16)°	(265 ± 10)°
$\alpha+1$	(161 ± 6)°	(309 ± 17)°	(71 ± 13)° / (201 ± 20)°	(298 ± 15)°
$\beta+1$	(226 ± 5)°	(180 ± 8)°	(183 ± 9)° / (225 ± 16)°	(176 ± 9)°
$\gamma+1$	(54 ± 3)°	(33 ± 11)°	(179 ± 9)° / (54 ± 13)°	(48 ± 11)°

<sup>a</sup>Average values as obtained from the six dinucleotide steps G5–G6, G8–G9, G11–G12, G17–G18, G20–G21 and G23–G24. <sup>b</sup>Average values as obtained from eight dinucleotide steps G2–G3, G3–G4, G8–G9, G9–G10, G14–G15, G15–G16, G20–G21 and G21–G22 in 1KF1 (7). <sup>c</sup>Parameters are listed for *anti-syn* and *syn-anti* steps of ZI phosphate conformation (41). <sup>d</sup>BI phosphate conformation (41).

These motifs could build upon the toolbox available for the construction of DNA assemblies (32). The topology of Z-G4 reveals novel folding principle of G-rich oligonucleotides that could be applied towards the design and prediction of G4 motifs. Furthermore, the compact structure of Z-G4 could facilitate its potential application as an aptamer for therapeutic or diagnostic purposes.

**Data deposition.** The coordinates of Z-G4 have been deposited in the Protein Data Bank (accession codes: 2MS9, NMR structure and 4U5M, crystal structure).

## METHODS

**Sample preparation.** The unlabeled and site-specific labeled DNA oligonucleotides were chemically synthesized on an ABI 394 DNA/RNA synthesizer. DNA sample concentrations were determined by measuring the UV absorbance at 260 nm.

**Circular dichroism.** Circular dichroism (CD) spectra were recorded at 25 °C using a JASCO-815 spectropolarimeter with a 1-cm path length quartz cuvette containing a solution volume of 500  $\mu$ L. Spectra (220 to 320 nm) were taken with a scan speed of 200 nm/min. DNA (~5  $\mu$ M) was dissolved in a buffer containing 70 mM KCl and 20 mM potassium phosphate, pH 7.0. For each measurement, an average of three scans was taken and the spectral contribution of the buffer was subtracted.

**NMR spectroscopy.** Unless otherwise stated, all NMR experiments were performed on 600 and 700 MHz Bruker spectrometers at 25 °C. The concentration of DNA samples was typically 0.1–2 mM. Solution contained 70 mM KCl, 20 mM potassium phosphate (pH 7.0) and 10% D<sub>2</sub>O. Spectral analyses were performed using SpinWorks software (<http://home.cc.umanitoba.ca/~wolowiec/spinworks/>), FELIX (Felix NMR, Inc.) and SPARKY (33) programs.

**NMR-restrained structure calculation.** Interproton distances for Z-G4 were classified based on NOESY experiments performed in D<sub>2</sub>O (mixing times, 100 and 300 ms) and H<sub>2</sub>O (mixing time, 200 ms). The structure of Z-G4 was calculated using XPLOR-NIH (34), AMBER 9.0 and 10.0 programs. Detailed procedures are described in the SI Appendix. Structures were displayed using PyMOL (35).

**Crystallization and X-ray crystallography.** Crystallization assays were performed by the sitting-drop methods, using a solution of Z-G4 (2 mM) in 10 mM potassium cacodylate buffer (pH 6.5) and 100 mM potassium chloride. Initial screening was done with the Matrix commercial screens (Hampton Research). Hexagonal crystals (spacegroup P3<sub>2</sub>1) were obtained using 35% methylpentanediol as precipitating agent, in the presence of 40 mM sodium cacodylate (pH 7.0), 20 mM magnesium chloride, 12 mM potassium chloride and 80 mM sodium chloride. For data collection, crystals were directly flash frozen in liquid nitrogen. Data were collected from a single crystal at the SOLEIL Proxima 1 beamline ( $\lambda = 0.979$  Å; Saint-Aubin, France) equipped with a Pilatus detector, and processed using XDS (36). Data collection statistics are summarized in Table 2. The structure was solved by molecular replacement, using PHASER (37) and data to 2.5 Å resolution. The coordinates of the G residues from the NMR structure were used as a search model. The model was then refined and completed with the T residues as well as ions and water molecules, by several cycles of manual building using Coot (38) and energy minimization using phenix.refine (39). In the last steps of refinement, anisotropic B factors were used. The final model contains all 28 residues of DNA, 4 potassium ions, 1 magnesium ion, and 94 water molecules, and has very good geometry (Table 2). A representative portion of the final electron density is illustrated in SI Appendix, Fig. S15.

**Structural analysis.** Structures were analyzed using an in-house script and Curves+ (40). The twist angle between two successive guanines was calculated as the angle between the vectors formed by the C8 atom coordinate and the middle point of the N1, C2 atom coordinates. The rise between two successive guanines was calculated as the distance between two averaged planes formed by the aromatics rings of guanine residues. Backbone dihedral angles were calculated using Curves+.

## ACKNOWLEDGEMENTS.

We thank Ngoc Quang Do and Eugene Choon Guobin for their participation in the early stages of the project, as well as the staff of the PROXIMA 1 beamline at SOLEIL for expert assistance during data collection. This work was supported by Singapore Ministry of Education Academic Research Fund Tier 3 (MOE2012-T3-1-001) and Tier 2 (MOE2012-T2-1-102), and grants from Nanyang Technological University to A.T.P., and by grants from the Centre National de la Recherche Scientifique and Ecole Polytechnique to the UMR7654 laboratory.

1. Watson JD & Crick FHC (1953) Molecular structure of nucleic acids: A structure for deoxyribose nucleic acid. *Nature* 171(4356):737–738.
2. Wang AHJ, et al. (1979) Molecular structure of a left-handed double helical DNA fragment at atomic resolution. *Nature* 282(5740):680–686.
3. Leontis NB, Stombaugh J, & Westhof E (2002) The non-Watson–Crick base pairs and their associated isosterism matrices. *Nucleic Acids Res.* 30(16):3497–3531.
4. Nikolova EN, et al. (2011) Transient Hoogsteen base pairs in canonical duplex DNA. *Nature* 470(7335):498–502.
5. Frank-Kamenetskii MD & Mirkin SM (1995) Triplex DNA Structures. *Annu. Rev. Biochem.* 64:65–95.
6. Smith FW & Feigon J (1992) Quadruplex structure of *Oxytricha* telomeric DNA oligonucleotides. *Nature* 356(6365):164–168.
7. Parkinson GN, Lee MPH, & Neidle S (2002) Crystal structure of parallel quadruplexes from human telomeric DNA. *Nature* 417(6891):876–880.
8. Gehring K, Leroy JL, & Guéron M (1993) A tetrameric DNA structure with protonated cytosine-cytosine base pairs. *Nature* 363(6429):561–565.
9. Lilley DMJ (2000) Structures of helical junctions in nucleic acids. *Q. Rev. Biophys.* 33(2):109–159.
10. Siddiqui-Jain A, Grand CL, Bearss DJ, & Hurley LH (2002) Direct evidence for a G-quadruplex in a promoter region and its targeting with a small molecule to repress c-MYC

transcription. *Proc. Natl. Acad. Sci. USA* 99(18):11593–11598.

11. Kumari S, Bugaut A, Huppert JL, & Balasubramanian S (2007) An RNA G-quadruplex in the 5' UTR of the NRAS proto-oncogene modulates translation. *Nat. Chem. Biol.* 3(4):218–221.
12. Cahoon LA & Seifert HS (2009) An alternative DNA structure is necessary for pilin antigenic variation in *Neisseria gonorrhoeae*. *Science* 325(5941):764–767.
13. Paeschke K, Capra JA, & Zakian VA (2011) DNA replication through G-quadruplex motifs is promoted by the *Saccharomyces cerevisiae* Pif1 DNA helicase. *Cell* 145(5):678–691.
14. Lopes J, et al. (2011) G-quadruplex-induced instability during leading-strand replication. *EMBO J.* 30(19):4033–4046.
15. Biffi G, Tannahill D, McCafferty J, & Balasubramanian S (2013) Quantitative visualization of DNA G-quadruplex structures in human cells. *Nat. Chem.* 5(3):182–186.
16. Maizels N & Gray LT (2013) The G4 genome. *PLoS Genet.* 9(4):e1003468.
17. Gellert M, Lipsett MN, & Davies DR (1962) Helix formation by guanylic acid. *Proc. Natl. Acad. Sci. USA* 48(12):2013–2018.
18. Adrian M, Heddi B, & Phan AT (2012) NMR spectroscopy of G-quadruplexes. *Methods* 57(1):11–24.
19. Trajkovski M, da Silva MW, & Plavec J (2012) Unique structural features of interconverting monomeric and dimeric G-quadruplexes adopted by a sequence from the intron of the N-myc gene. *J. Am. Chem. Soc.* 134(9):4132–4141.
20. Yatsunyk LA, Mendoza O, & Mergny JL (2014) "Nano-oddities": Unusual nucleic acid

545  
546  
547  
548  
549  
550  
551  
552  
553  
554  
555  
556  
557  
558  
559  
560  
561  
562  
563  
564  
565  
566  
567  
568  
569  
570  
571  
572  
573  
574  
575  
576  
577  
578  
579  
580  
581  
582  
583  
584  
585  
586  
587  
588  
589  
590  
591  
592  
593  
594  
595  
596  
597  
598  
599  
600  
601  
602  
603  
604  
605  
606  
607  
608  
609  
610  
611  
612

- assemblies for DNA-based nanostructures and nanodevices. *Acc. Chem. Res.* 47:1836–1844.
21. Bates PJ, Laber DA, Miller DM, Thomas SD, & Trent JO (2009) Discovery and development of the G-rich oligonucleotide AS1411 as a novel treatment for cancer. *Exp Mol Pathol* 86(3):151–164.
  22. Dailey MM, Miller MC, Bates PJ, Lane AN, & Trent JO (2010) Resolution and characterization of the structural polymorphism of a single quadruplex-forming sequence. *Nucleic Acids Res.* 38(14):4877–4888.
  23. Vorlíčková M, Kejnovská I, Bednářová K, Renčíuk D, & Kypr J (2012) Circular dichroism spectroscopy of DNA: From duplexes to quadruplexes. *Chirality* 24(9):691–698.
  24. Lech CJ, Heddi B, & Phan AT (2013) Guanine base stacking in G-quadruplex nucleic acids. *Nucleic Acids Res.* 41(3):2034–2046.
  25. Do NQ & Phan AT (2012) Monomer–dimer equilibrium for the 5'–5' stacking of propeller-type parallel-stranded G-quadruplexes: NMR structural study. *Chem. Eur. J.* 18(46):14752–14759.
  26. Pohl FM & Jovin TM (1972) Salt-induced co-operative conformational change of a synthetic DNA: Equilibrium and kinetic studies with poly(dG-dC). *J. Mol. Biol.* 67(3):375–396.
  27. Phan AT, et al. (2011) Structure-function studies of FMRP RGG peptide recognition of an RNA duplex-quadruplex junction. *Nat. Struct. Mol. Biol.* 18(7):796–804.
  28. Huang H, et al. (2014) A G-quadruplex-containing RNA activates fluorescence in a GFP-like fluorophore. *Nat. Chem. Biol.* 10(8):686–691.
  29. Warner KD, et al. (2014) Structural basis for activity of highly efficient RNA mimics of green fluorescent protein. *Nat. Struct. Mol. Biol.* 21(8):658–663.
  30. Tran PLT, Moriyama R, Maruyama A, Rayner B, & Mergny JL (2011) A mirror-image tetramolecular DNA quadruplex. *Chem. Commun.* 47(19):5437–5439.
  31. Virgilio A, et al. (2011) Unprecedented right- and left-handed quadruplex structures formed by heterochiral oligodeoxyribonucleotides. *Biochimie* 93(7):1193–1196.
  32. Seeman NC (2010) Nanomaterials Based on DNA. *Annu. Rev. Biochem.* 79:65–87.
  33. Goddard TD & Kneller DG (*SPARKY 3* (University of California, San Francisco, California).)
  34. Schwieters CD, Kuszewski JJ, Tjandra N, & Clore GM (2003) The Xplor-NIH NMR molecular structure determination package. *J. Magn. Reson.* 160(1):65–73.
  35. DeLano WL & Bromberg S (2004) *PyMOL User's Guide* (DeLano Scientific LLC, San Carlos, California.).
  36. Kabsch W (2010) *XDS*. *Acta Crystallogr. D* 66(Pt 2):125–132.
  37. McCoy AJ, et al. (2007) *Phaser* crystallographic software. *J. Appl. Cryst.* 40(Pt 4):658–674.
  38. Emsley P, Lohkamp B, Scott WG, & Cowtan K (2010) Features and development of *Coot*. *Acta Crystallogr. D* 66(Pt 4):486–501.
  39. Afonine PV, et al. (2012) Towards automated crystallographic structure refinement with *phenix.refine*. *Acta Crystallogr. D* 68(Pt 4):352–367.
  40. Lavery R, Moakher M, Maddocks JH, Petkeviciute D, & Zakrzewska K (2009) Conformational analysis of nucleic acids revisited: Curves+. *Nucleic Acids Res.* 37(17):5917–5929.

613  
614  
615  
616  
617  
618  
619  
620  
621  
622  
623  
624  
625  
626  
627  
628  
629  
630  
631  
632  
633  
634  
635  
636  
637  
638  
639  
640  
641  
642  
643  
644  
645  
646  
647  
648  
649  
650  
651  
652  
653  
654  
655  
656  
657  
658  
659  
660  
661  
662  
663  
664  
665  
666  
667  
668  
669  
670  
671  
672  
673  
674  
675  
676  
677  
678  
679  
680

# Submission PDF